Thermodynamic Characterization of Triheme Cytochrome PpcA from *Geobacter sulfurreducens*: Evidence for a Role Played in e^-/H^+ Energy Transduction[†,‡]

Miguel Pessanha,[§] Leonor Morgado,[§] Ricardo O. Louro,[||] Yuri Y. Londer,[⊥] P. Raj Pokkuluri,[⊥] Marianne Schiffer,[⊥] and Carlos A. Salgueiro*[,§]

Requimte, CQFB, Departamento de Química, Faculdade de Ciências e Tecnologia, Universidade Nova de Lisboa, Quinta da Torre, 2829-516 Caparica, Portugal, Instituto de Tecnologia Química e Biológica, Universidade Nova de Lisboa, Rua da Quinta Grande 6, 2780-156 Oeiras, Portugal, and Biosciences Division, Argonne National Laboratory, Argonne, Illinois 60439

Received July 11, 2006; Revised Manuscript Received September 13, 2006

ABSTRACT: The facultative aerobic bacterium *Geobacter sulfurreducens* produces a small periplasmic *c*-type triheme cytochrome with 71 residues (PpcA) under anaerobic growth conditions, which is involved in the iron respiration. The thermodynamic properties of the PpcA redox centers and of a protonatable center were determined using NMR and visible spectroscopy techniques. The redox centers have negative and different reduction potentials (−162, −143, and −133 mV for heme I, III, and IV, respectively, for the fully reduced and protonated protein), which are modulated by redox interactions among the hemes (covering a range from 10 to 36 mV) and by redox−Bohr interactions (up to −62 mV) between the hemes and a protonatable center located in the proximity of heme IV. All the interactions between the four centers are dominated by electrostatic effects. The microscopic reduction potential of heme III is the one most affected by the oxidation of the other hemes, whereas heme IV is the most affected by the protonation state of the molecule. The thermodynamic properties of PpcA showed that pH strongly modulates the redox behavior of the individual heme groups. A preferred electron transfer pathway at physiologic pH is defined, showing that PpcA has the necessary thermodynamic properties to perform e^-/H^+ energy transduction, contributing to a H^+ electrochemical potential gradient across the periplasmic membrane that drives ATP synthesis. PpcA is 46% identical in sequence to and shares a high degree of structural similarity with a periplasmic triheme cytochrome c_7 isolated from *Desulfuromonas acetoxidans*, a bacterium closely related to the Geobacteracea family. However, the results obtained for PpcA are quite different from those published for *D. acetoxidans* c_7, and the physiological consequences of these differences are discussed.

Geobacter spp. are microorganisms of the Geobacteracea family that display a considerable respiratory versatility. In addition to more common soluble electron acceptors such as fumarate, these bacteria have the ability to reduce soluble toxic metal oxides of Cr(VI) and radioactive contaminants like U(VI) to the corresponding insoluble forms [Cr(III) and U(IV), respectively] (*1*, *2*). The flexibility presented by *Geobacter* toward different electron acceptors is further extended to the reduction of insoluble metal oxides [Fe(III)] coupled to the oxidation of organic carbon [for reviews, see the work of Lovley (*3*, *4*)]. These observations had a considerable impact on the bioremediation field, since they prompted the proposal of new strategies for cleaning of environments contaminated with toxic compounds such as soluble toxic metals and radionuclides (*1*, *2*, *5*, *6*). The unusual competence of *Geobacter* bacteria to efficiently reduce metal ions as part of its bioenergetic metabolism might be due to the presence of more than 100 *c*-type cytochromes as revealed by the examination of the complete genome of *Geobacter sulfurreducens* (*7*). Several *Geobacter* cytochromes are mainly expressed during growth in the presence of insoluble Fe(III) oxides as electron acceptors, and their participation in this metabolic pathway is corroborated by gene-knockout experiments, which showed that growth in the presence of insoluble Fe(III) was impaired or greatly inhibited when some of these multiheme cytochromes were disrupted (*8*−*10*). One such protein is PpcA,[1] a periplasmic triheme *c*-type cytochrome (*10*). This is also the

[†] This work is supported by Fundação para a Ciência e Tecnologia (FCT) by Project Grants POCI/QUI/60060/2004 and POCI/BIO/58652/2004 and by the U.S. Department of Energy's Office of Science, Biological and Environmental Research NABIR and GTL programs under Contract W-31-109-Eng-38. M.P. acknowledges Fundação para a Ciência e Tecnologia (FCT), Portugal, for Postdoctoral Grant BPD/20571/2004.

[‡] We dedicate this article to the memory of Professor António V. Xavier (1943−2006), who among many other important scientific achievements had an outstanding contribution to the understanding of the role played by multiheme cytochromes in energy transduction mechanisms.

* To whom correspondence should be addressed: Departamento de Química, Faculdade de Ciências e Tecnologia, Universidade Nova de Lisboa, Quinta da Torre, 2829-516 Caparica, Portugal. Telephone: (351) 212 948 300. Fax: (351) 212 948 385. E-mail: csalgueiro@dq.fct.unl.pt.

[§] Faculdade de Ciências e Tecnologia, Universidade Nova de Lisboa.

[||] Instituto de Tecnologia Química e Biológica, Universidade Nova de Lisboa.

[⊥] Argonne National Laboratory.

[1] Abbreviations: PpcA, *G. sulfurreducens* triheme cytochrome; Dac_7, *D. acetoxidans* triheme cytochrome; EXSY, two-dimensional exchange spectroscopy.

10.1021/bi061394v CCC: $33.50
Published on Web 10/28/2006

case for the outer-membrane cytochromes OmcG and OmcH (*11*), the dodecaheme cytochrome OmcB (*9*), the tetraheme cytochromes OmcD and OmcE, and the hexaheme cytochrome OmcS (*12*, *13*). Also, the diheme *c*-type cytochrome which is predicted to be localized in the periplasm and possibly loosely associated with the inner membrane designated as MacA is shown to be involved in the Fe(III) reduction pathways (*8*, *10*, *12*). On the basis of the reported cytochrome location within the cell, a model for sequential electron flow among the cytochromes involved in iron respiration was proposed (*12*, *14*). However, the sequential tracing of the various components in this pathway has not yet been fully established.

Despite the unquestionable importance of multiheme cytochromes in the metabolic pathways of *Geobacter*, particularly in those that lead to metal reduction, little is known about the functionality of the individual electron transfer proteins, and therefore about the electron transfer mechanisms in these bacteria. From all the cytochromes mentioned above that participate in the Fe(III) reduction, a three-dimensional structure was determined only for PpcA (*15*), and preliminary insights into its redox behavior were obtained (*16*).

The amino acid sequence of PpcA is 46% identical with that of the triheme cytochrome isolated from *Desulfuromonas acetoxidans* (*17*), a bacterium closely related to the Geobacteracea family. The available structural data for *D. acetoxidans* triheme cytochrome, Dac_7 (*18*, *19*), also show that this cytochrome and PpcA are structurally similar (*15*). The heme core architecture is conserved in both proteins and closely related to those of tetraheme cytochrome c_3 species isolated from the Desulfovibrionacea family [for a review, see Bento et al. (*20*)], except for heme II which is not present in the triheme proteins. Thus, to be consistent with the literature, the heme groups of PpcA are numbered I, III, and IV by analogy to the structurally homologous hemes in tetraheme cytochrome c_3 (Roman numerals indicating the heme by the order of attachment to the CXXCH motif in the polypeptide chain). Dac_7 and PpcA are abundantly produced in their cells, and both are expected to play a fundamental role in the bioenergetic pathways of these bacteria. A detailed thermodynamic characterization of the redox centers of Dac_7 was previously carried out (*21*). A preliminary analysis of the redox behavior of PpcA hinted at differences between the two proteins (*16*), and the work presented here reports a complete thermodynamic characterization of the individual redox centers of PpcA, which is discussed in the framework of its functional and physiological implications.

MATERIALS AND METHODS

Cell Growth and Protein Purification. *G. sulfurreducens* triheme cytochrome (PpcA) was produced in *Escherichia coli* and purified by cation exchange and gel filtration columns as described previously (*15*, *22*).

NMR Sample Preparations. The protein was lyophilized twice with ^2H_2O (99.9 at. %) and then dissolved in 600 μL of the same solvent to a final concentration of approximately 70 μM, calculated using the specific absorption coefficient of the α band of the reduced form for PpcA (97.5 mM^{-1} cm^{-1}) as determined by Seeliger et al. (*23*). NMR spectra were obtained before and after the lyophilization, to confirm that the protein integrity was not affected. The ionic strength was adjusted to 500 mM by addition of NaCl prepared in ^2H_2O. The pH was adjusted by addition of small amounts of NaO^2H or ^2HCl.

Complete reduction of the samples were achieved by the reaction with gaseous hydrogen in the presence of catalytic amounts of the enzyme Fe-hydrogenase, isolated from *Desulfovibrio vulgaris* (Hildenborough). Partially oxidized samples were obtained by flushing out the hydrogen from the reduced sample with argon followed by the addition of controlled amounts of air to the NMR tube. In the reduced and intermediate stages of oxidation, the pH was adjusted inside an anaerobic glove chamber (Mbraun MB 150 I) with argon circulation to prevent reoxidation of the sample. The pH values reported in this work are direct meter readings.

NMR Experiments. All NMR spectra were recorded on a Bruker DRX500 spectrometer equipped with a BBI-XYZ 5 mm inverse detection probe head with internal B_0 gradient coils and a Eurotherm 818 temperature control unit. In a previous work, NMR experiments performed at 274 K with an ionic strength of 500 mM and 500 μM PpcA samples allowed the determination of the order of oxidation of PpcA heme groups (*16*). However, the determination of the absolute values for the redox potentials and interactions requires redox titrations followed by visible spectroscopy in addition to NMR data (see Thermodynamic Model), which are experimentally challenging at very low temperatures (e.g., 274 K) due to the very slow response of the electrode. To overcome this difficulty, in the work presented here, the temperature was increased to 288 K, and to slow intermolecular electronic exchange on the NMR time scale, the protein samples were diluted to 70 μM. The redox patterns of heme methyl groups $12^1CH_3^I$, $7^1CH_3^{III}$, and $12^1CH_3^{IV}$ (*16*) were used as guide to map the individual heme oxidation patterns in two-dimensional (2D) exchange spectroscopy (EXSY) NMR spectra at 288 K. For each pH value, a series of 2D EXSY NMR experiments with the sample poised at several degrees of oxidation are conducted to unambiguously map the oxidation of the individual hemes throughout the redox titrations. All the 2D EXSY NMR experiments were conducted with a mixing time of 25 ms and by recording 4096 (t_2) $\times$ 256 (t_1) data points to cover a sweep width of 22.5 kHz, with at least 256 scans per increment. The NMR spectra were calibrated using the water signal as an internal reference, and the proton chemical shifts are reported relative to tetramethylsilane.

Redox Titrations Followed by Visible Spectroscopy. Anaerobic redox titrations of 18 μM PpcA solutions in 500 mM TRIS/maleate buffer (pH 6.9 and 7.9) at 288 K were performed as previously described (*24*). To check for hysteresis, each redox titration was performed in both oxidative and reductive directions. To ensure a good equilibrium between the redox centers and the working electrode, a mixture of the following redox mediators at a final concentration of 4 μM was added to the protein solution: methylene blue, gallocyanine, indigo tetrasulfonate, indigo trisulfonate, indigo disulfonate, anthraquinone-2,7-disulfonate, 2-hydroxy-1,4-naphthoquinone, anthraquinone-2-sulfonate, safranine O, diquat, benzyl viologen, neutral red, and methyl viologen. A combined Pt/Ag/AgCl electrode calibrated with saturated quinhydrone solutions at pH 7.0 and

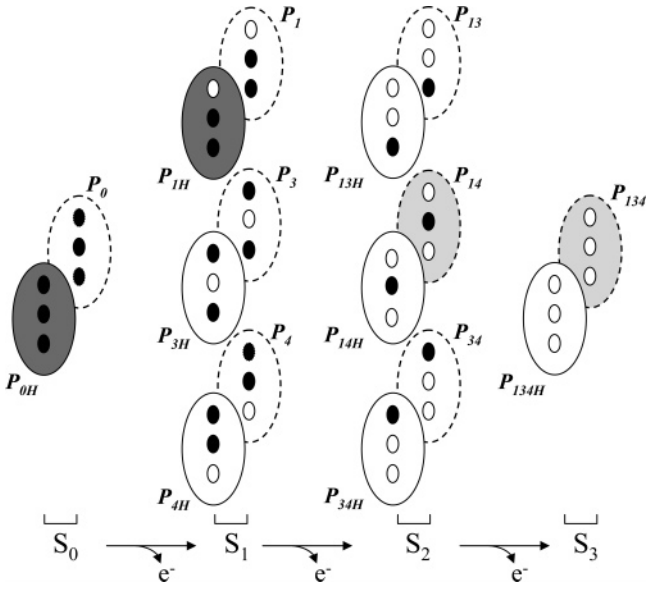

FIGURE 1: Electronic distribution scheme for a triheme cytochrome with a proton-linked equilibrium showing the 16 possible microstates. The three inner circles represent the hemes which can be either reduced (black) or oxidized (white). The outer circles with solid and dashed lines represent the protonated and deprotonated microstates, respectively. The microstates are grouped, according to the number of oxidized hemes, in four oxidation stages (S_{0-3}) connected by one electron step. P_{0H} and P_0 represent the reduced protonated and deprotonated microstates, respectively. P_{ijkH} and P_{ijk} represent the protonated and deprotonated microstates, respectively, where *i*−*k* represent the heme(s) that are oxidized in that particular microstate. The microstates with gray background are those functionally relevant as revealed in this study (see Results and Discussion).

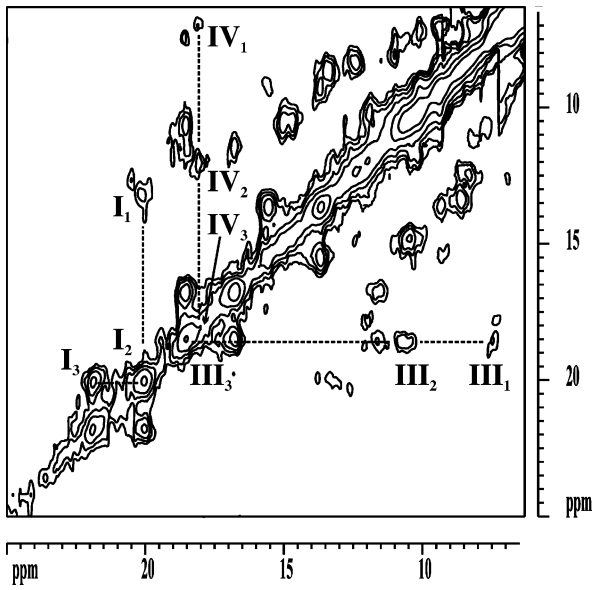

FIGURE 2: Portion of a typical 2D EXSY spectrum of partially oxidized PpcA obtained at pH 6.3 and 288 K. Cross-peaks connecting the signals of heme methyls $12^1CH_3^I$, $7^1CH_3^{III}$, and $12^1CH_3^{IV}$ in different oxidation stages (3, 2, and 1) are denoted with dashed lines. The Roman and Arabic numbers indicate the heme groups and the oxidation stages, respectively.

4.0 were used to measure the solution potentials, and the visible spectra were recorded at 288 K in a Shimadzu UV-1203 spectrophotometer, placed inside the anaerobic chamber with O_2 levels kept below 0.5 ppm. The reduced fraction of PpcA was determined using the α band peak ($\lambda = 551$ nm). The optical contribution of the mediators was subtracted by measuring the height of the peak at 551 nm relative to the straight line connecting the two isosbestic points ($\lambda = 541$ and 559 nm) flanking the α band according to the method described in the literature (*24*). Each experiment was performed at least twice.

Thermodynamic Model. For the thermodynamic characterization of PpcA redox centers, we used a model for interacting charged centers that has been used for several multiheme proteins containing up to six interacting centers (*21*, *24*−*28*). In the particular case of a triheme cytochrome, three consecutive reversible steps of one-electron transfer convert the fully reduced state (stage 0) into the fully oxidized state (stage 3), and therefore, four different redox stages can be defined, each grouping microstates with the same number of oxidized hemes (Figure 1). Additionally, within each microstate, the group responsible for the redox−Bohr effect may be protonated or deprotonated, leading to a total of 16 microstates (Figure 1). Obviously, once the oxidation degree of two of the hemes at each oxidation stage is known, together with the overall oxidation of the protein, the degree of oxidation of the third heme is determined, and therefore, there is redundancy when data for all three hemes are collected. If the intramolecular electronic exchange is fast and the intermolecular electronic exchange is slow on the NMR time scale, each heme substituent at the four oxidation stages will give rise to a separate set of resonances, as in the case of PpcA (Figure 2). The paramagnetic chemical shifts of these resonances are proportional to the degree of oxidation of that particular heme and can be used to monitor the oxidation of the heme throughout the redox titration (*29*−*31*). Under such experimental conditions, there are enough data to define parameters of the model which, for the simplest case of three hemes and one protonatable center, can be described by 10 parameters: three heme reduction potentials, the deprotonation energy of the protonatable center, three redox interactions between the heme groups, and three interactions between the hemes and the protonatable center (redox−Bohr interactions). These parameters can be unambiguously obtained by combining NMR and visible spectroscopy data obtained at various degrees of oxidation and at various solution pH values [for details, see Turner et al. (*31*)]. Fitting of the model to the NMR and visible data was performed simultaneously using the Marquardt method. The experimental uncertainty of the NMR data was evaluated from the line width of each NMR signal at half-height, and the visible data points were given with an uncertainty of 3% of the total optical signal.

RESULTS AND DISCUSSION

The pH dependence of the paramagnetic chemical shifts of heme methyl groups $12^1CH_3^I$, $7^1CH_3^{III}$, and $12^1CH_3^{IV}$ in the pH range of 5.7−9.2 and the data obtained for redox titrations followed by visible spectroscopy at pH 6.9 and 7.9 were used to monitor the thermodynamic properties of PpcA. The fittings of both NMR and visible data with the thermodynamic model are reported in Figures 3 and 4, respectively. The thermodynamic parameters obtained for PpcA are listed in Table 1, together with the macroscopic pK_a values associated with each of the four stages of oxidation. The redox titrations, followed by visible spectroscopy at pH 6.9 and 7.9, show an approximately 20 mV

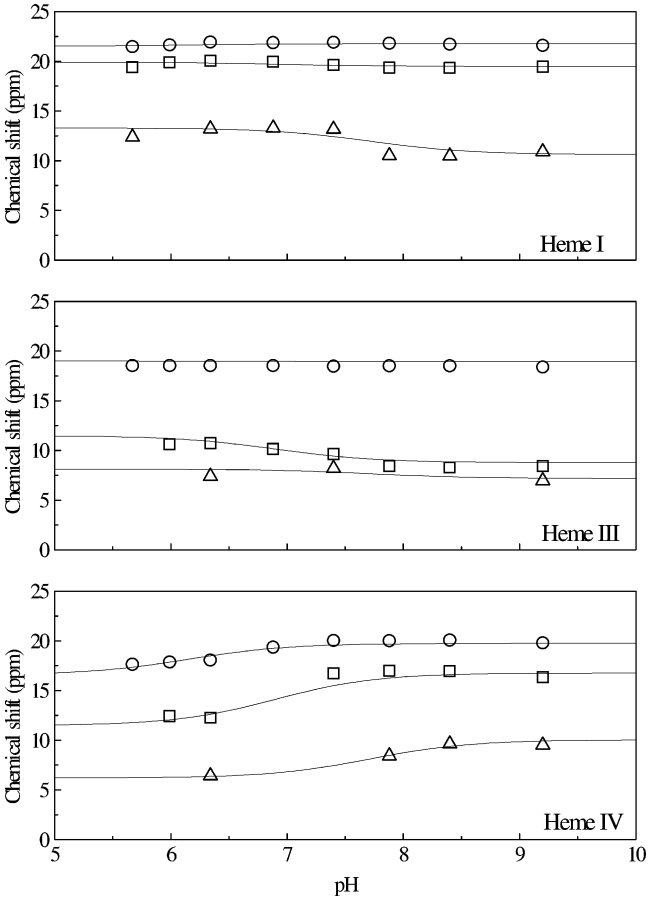

FIGURE 3: pH dependence of the chemical shift of heme methyl group resonances $12^1CH_3^I$, $7^1CH_3^{III}$, and $12^1CH_3^{IV}$ of PpcA. Upward-pointing triangles correspond to stage 1 of oxidation, squares to stage 2, and circles to stage 3. The chemical shifts of the heme methyl groups in fully reduced stage 0 are not plotted since they are unaffected by pH. They are 2.63 ($12^1CH_3^I$), 4.22 ($7^1CH_3^{III}$), and 4.04 ppm ($12^1CH_3^{IV}$).

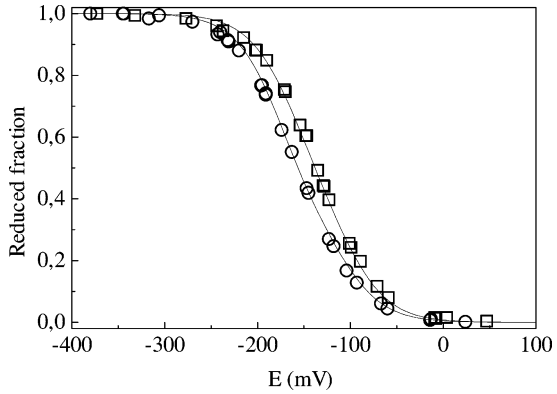

FIGURE 4: Reduced fraction of PpcA determined by visible spectroscopy at pH 6.9 (□) and 7.9 (○) at 288 K. The solid lines are the result of the simultaneous fitting of the NMR and visible data (see Materials and Methods).

separation (Figure 4), leading to a significant redox−Bohr effect of 2.3 pH units between the fully reduced and fully oxidized protein pK_a values (Table 1B). These redox curves are identical to those obtained at 298 K (*16*), showing that the PpcA macroscopic reduction potentials are pH-dependent and unaffected within this temperature range.

Figures 3 and 4 show that the features of the experimental data are captured well by the thermodynamic model, with the fitted curves following closely the experimental data.

Table 1: Thermodynamic Parameters Determined for PpcA by Fitting the NMR and Visible Data to the Model of Four Charged Interacting Centers[a]

A

	energy (meV)			
	heme I	heme III	heme IV	protonatable center
heme I	**−162 (6)**	27 (3)	10 (3)	−34 (5)
heme III		**−143 (6)**	36 (3)	−35 (5)
heme IV			**−133 (6)**	−62 (5)
protonatable center				**482 (11)**

B

	stage 0	stage 1	stage 2	stage 3
pK_a	8.4	7.7	6.9	6.1

[a] In part A, the boldface values represent the oxidation energies of the three hemes and the deprotonating energies for the protonatable center in the fully reduced and protonated protein. The lightface values represent the redox and redox−Bohr interaction energies among the four centers. Standard errors are given in parentheses. Part B lists PpcA macroscopic pK_a values for the four stages of oxidation, from the fully reduced protein (stage 0) to the fully oxidized protein (stage 3).

Some data points are not reported due to excessive line broadening, making their measurement highly uncertain. The low values of the standard errors of the thermodynamic parameters that were obtained (Table 1) are also a good indication that the parameters are all defined well by the experimental data. Table 1 shows that the microscopic reduction potentials of each heme are negative, as expected from their considerable exposure to the solvent and from the bis-histidinyl axial coordination [for a review, see Dolla et al. (*32*)]. The interaction energy for each pair of hemes is positive, indicating that the oxidation of a particular heme renders the oxidation of its neighbors more difficult (negative homocooperativity). On the other hand, the interaction energies between the hemes and the protonatable center are negative (positive heterocooperativity); i.e., the oxidation of the hemes facilitates the deprotonation of the protonatable center and vice versa. Both the homotropic (heme redox interations) and heterotropic (redox−Bohr interactions) cooperativities change the affinity of the hemes and the protonatable center in the sense expected on electrostatic grounds (*33*). The values for the redox−Bohr interactions suggest that the dominant protonatable group is close to heme IV because this is the heme that exhibits the greastest pH dependence in the reduction potential (Table 1). It is most likely one of its propionate groups since the magnitude of the redox−Bohr interaction with heme IV is similar to those reported in the literature for *D. vulgaris* (Hildenborough) and *Desulfovibrio gigas* where propionate 13 was shown to be the dominant redox−Bohr group (*34*, *35*).

The analysis of the relative microscopic reduction potentials of each heme group (Table 1A) shows that heme I has the lowest affinity for electrons in the reduced and protonated protein, followed by hemes III and IV. However, the homocooperativities between the heme groups alter their electron affinity as oxidation progresses such that their individual titration curves are substantially different from a Nernst curve of isolated centers. Therefore, the actual order of the midpoint reduction potentials is as follows: I, IV, and III. The profile of oxidation of the heme groups covering the physiological pH range is shown in Figure 5. Crossovers

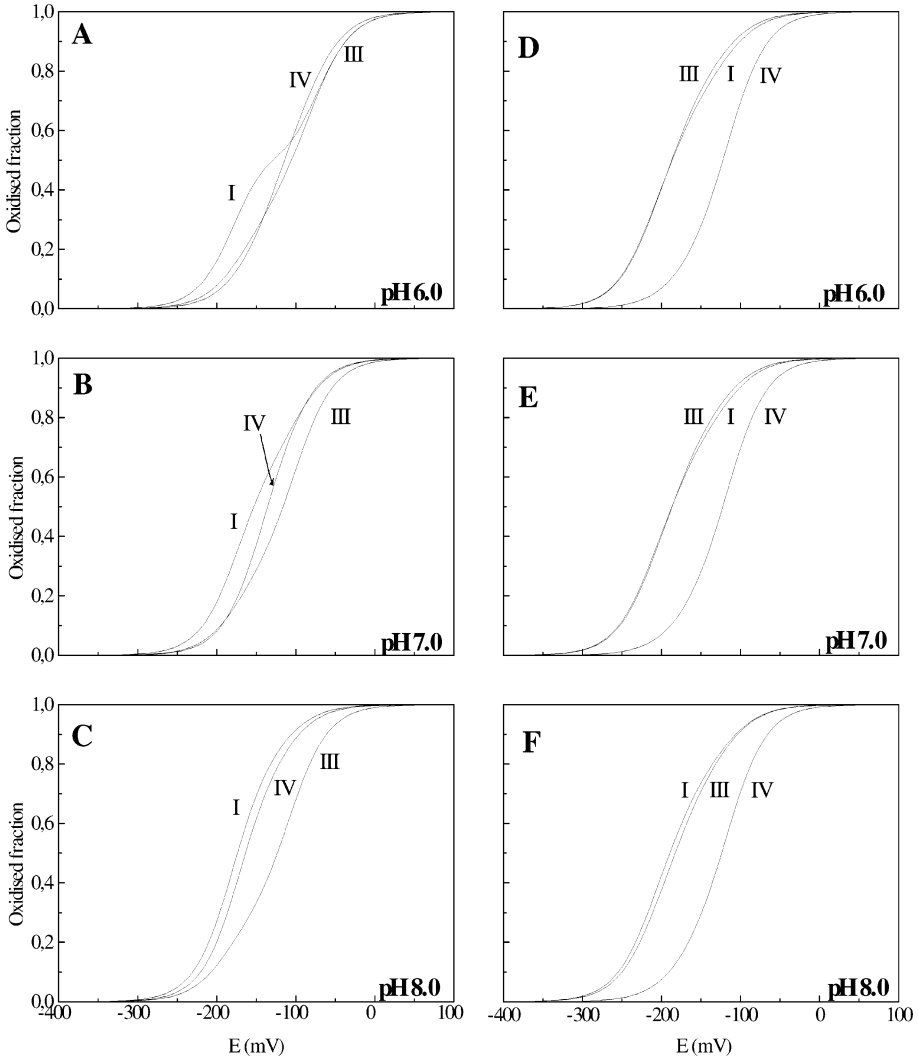

FIGURE 5: Oxidized fractions of the individual hemes of PpcA (A−C) and *Dac*$_7$ (D−F) at different pH values. The PpcA heme oxidation curves were calculated as a function of the solution reduction potential using the parameters listed in Table 1, whereas those of *Dac*$_7$ heme were calculated from the thermodynamic parameters determined by Correia et al. (*21*).

between the individual curves at pH 6 and 7 (Figure 5A,B) clearly indicate that the affinity for an electron of each redox center is tuned by neighboring heme groups. The oxidation profiles of the individual hemes obtained at different pH values (Figure 5) also show that the redox behavior of PpcA is clearly modulated by the pH. The titration curve of heme I is dramatically different from a Nernst curve of isolated centers, which becomes less pronounced at higher pH values. The behavior observed for higher pH values is easily explained by the network of redox−Bohr interactions. Indeed, for the deprotonated protein, the heme reduction potentials of hemes I (−196 mV) and IV (−195 mV) become very similar and significantly lower from that of heme III (−178 mV), when compared with those for the reduced protonated protein (Table 1). Given the separation of heme I and IV microscopic reduction potentials from that of heme III at high pH values, and since the redox interaction between these two hemes is relatively weak (10 mV), the oxidation of these heme groups is not significantly affected by the oxidation of heme III, and thus, crossover of the individual heme oxidation curves is not observed (Figure 5C). On the contrary, lowering the pH makes the individual heme reduction potentials closer to each other, leading to crossover of the curves, so that all three hemes titrate in a similar range of solution potentials at the end of oxidation (Figure 5A). The individual heme behavior described above for PpcA contrasts drastically with the results obtained for its homologous *Dac*$_7$ obtained under the same experimental conditions (*21*). Indeed, the oxidation profile of the individual hemes in *Dac*$_7$ at pH 6.0, 7.0, and 8.0 (panels D−F of Figure 5, respectively) is virtually unaffected.

The effect of the pH in the PpcA heme redox behavior can be analyzed at the level of the microstate populations at intermediate oxidation stages (Figure 6). At physiologic pH (pH 7.0), stage 0 is dominated by the protonated form P_{0H} and stage 1 is dominated by the oxidation of heme I (P_{1H}) while keeping the acid−base center protonated. Stage 2 is dominated by the oxidation of hemes I and IV and deprotonation of the acid−base center (P_{14}), which remains deprotonated in stage 3 (P_{134}). This coupled binding of electrons and protons is lost at both pH 6 and 8 as shown in Figure 6. Therefore, at pH 7.0 a route is defined for the electrons within PpcA: $P_{0H} \rightarrow P_{1H} \rightarrow P_{14} \rightarrow P_{134}$ (Figures 1 and 7); at other pH values, there is no coherent path. Moreover, it is clear from the analysis of Figure 6 that in association with the favored electron transfer pathway at physiologic pH, a deprotonation occurs as one electron is transferred between oxidation stages 1 and 2 (Figure 1). Thus,

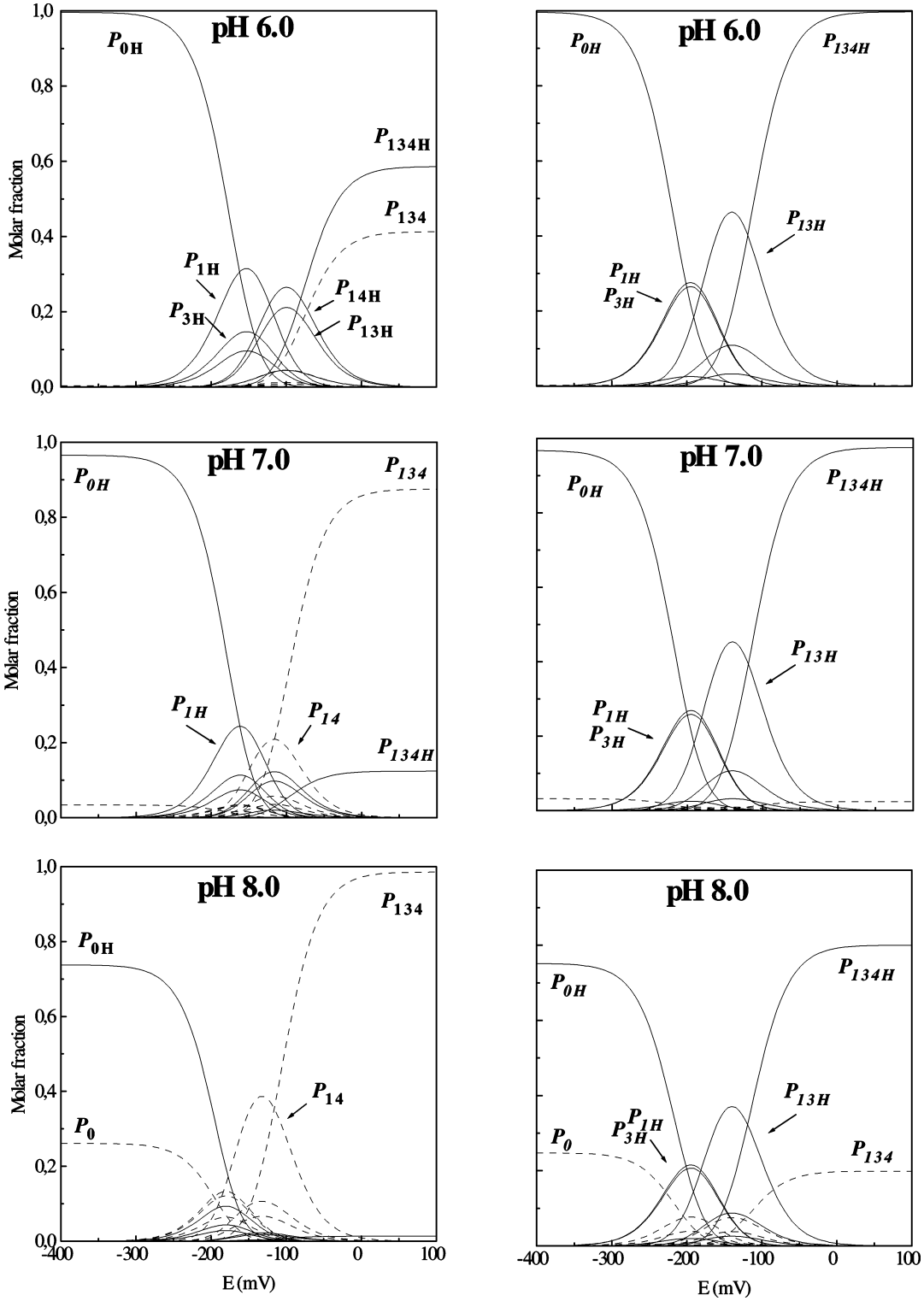

FIGURE 6: Molar fraction of the 16 individual microstates (see Figure 1) of PpcA (left) and Dac_7 (right) at different pH values. The PpcA curves were calculated as a function of the solution reduction potential using the parameters listed in Table 1, whereas those of Dac_7 heme were calculated from the thermodynamic parameters determined by Correia et al. (*21*). Solid and dashed lines indicate the protonated and deprotonated microstates, respectively. For clarity, only the relevant microstates are labeled.

a deprotonated microstate of PpcA (P_{14}) in oxidation stage 2 is ready to receive electrons and protons from a partner, originating a protonated microstate (P_{1H}) of stage 1 (Figure 7). This functional behavior of PpcA is schematically depicted in Figure 7, showing how selected microstates could confer directionality of events. (i) Uptake of a strongly reducing electron (−185 mV) can be followed by uptake of a weakly acidic proton (pK_a = 7.8) in the pH range of 6.8−7.8 from stage 2 to stage 1. (ii) When it meets its physiological downstream redox partner, donation of less reducing electrons (−123 mV) elicits the release of a more acidic proton (pK_a = 6.8) in the periplasm. Simple charge compensation could be achieved without this intricate sequence of events. This functional aptitude is completely different from what is observed with the homologous Dac_7. In this case, no preferential path for electron transfer is

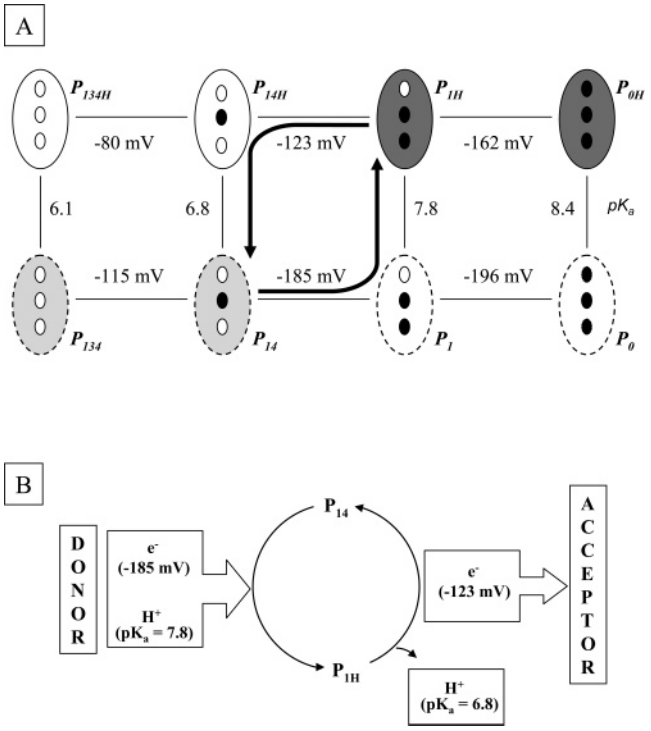

FIGURE 7: Thermodynamic and mechanistic bases for energy transduction by PpcA. (A) The functional pathway is also drawn with arrows in this scheme. The donor supplies PpcA with electrons which assist the proton uptake. The energy transduction facilitates the release of lowered pK_a protons in the periplasm with the concomitant transfer of electrons to the acceptor. (B) Energy transduction mechanism achieved between oxidation stages 1 and 2 and involving microstates P_{1H} and P_{14}.

achieved and no electron/proton transfer coupling in the pH range of 6−8 is attained (Figure 6). These dramatic differences in the redox behavior of these two homologue cytochromes must account for their different physiological function. Interestingly, it is the heme that is more affected by the acid−base center (heme IV) that dominates the redox transitions from stage 1 to stage 2, and the magnitude of the redox−Bohr interaction is in the range reported in the literature for the coupling with one of the propionates of the heme (*31*, *33*−*37*). The vicinity of heme IV is dominated by lysine residues that form an anion binding region where a sulfate was found in the crystallographic structure (*15*). In the homologous *Dac*$_7$, this is also the binding region for chromate (*38*), therefore establishing the importance of this area for electron transfer.

It was recently shown that for growth in the presence of Fe(III) as an electron acceptor the bacterium *G. sulfurreducens* needs additional e^-/H^+ coupling mechanisms in comparison to those used in fumarate respiration (*39*). As suggested by the authors, the most likely mechanism for additional membrane potential generation is coupling of electron transfer to the periplasmic cytochromes involved in the Fe(III) reduction with proton translocation so that additional membrane potential can be generated for ATP production. Thus, since PpcA is a periplasmic cytochrome that participates in the Fe(III) reduction pathways (*10*) and from the thermodynamic properties determined in this work, it can be proposed that PpcA is the coupling protein performing energy transduction after receiving e^- and H^+ from the redox partner(s) (Figure 7). As a consequence, protons are acidified and released in the periplasmic space, contributing to ATP synthesis, whereas the de-energization of the electrons would commit them to the pathways involved in Fe(III) reduction, preventing back flow and reinforcing the directionality of electron transfer within the respiratory chain.

CONCLUSIONS

The thermodynamic results obtained for PpcA and the important homo- and heterocooperativities displayed by heme III and IV indicate that these hemes play an important role in the redox cycle of this electron transfer protein. Taken together, the thermodynamic parameters obtained for PpcA showed that this protein is designed to present a preferential electron transfer pathway at physiologic pH coupled with proton transfer. Comparison of the results obtained for PpcA with those obtained for the homologous *Dac*$_7$ in ref *21* showed that although they are 46% identical in sequence and have a conserved structural motif (*15*, *18*), the two cytochromes have remarkable thermodynamic properties and functional differences, being an excellent example of how structurally related proteins can present functional differences that lead to distinct physiological roles.

Having a well-defined functional electron transfer pathway between oxidation stages 1 and 2, PpcA appears to be designed to functionally work with specific electron donors and acceptors involving both electron and proton transfer, thus contributing to the energy transduction cycle that leads to cellular ATP production. This is the first experimental evidence of a e^-/H^+ energy transduction in the periplasmic space of *G. sulfurreducens*. This coupling was recently proposed as being essential in supporting energy generation when using Fe(III) as a terminal electron acceptor (*39*). Experiments to test whether PpcA participates in this process are to be pursued.

Further detailed studies of the various proteins and complexes involved in the Fe(III) reduction pathway in *G. sulfurreducens* will allow the modeling of the metabolic flow and eventually manipulation for optimization of important applications such as bioremediation and electricity generation.

ACKNOWLEDGMENT

We are very grateful to Prof. David L. Turner for helpful discussions on thermodynamic modelling.

REFERENCES

1. Lloyd, J. R., and Lovley, D. R. (2001) Microbial detoxification of metals and radionuclides, *Curr. Opin. Biotechnol. 12*, 248−253.
2. Anderson, R. T., Vrionis, H. A., Ortiz-Bernad, I., Resch, C. T., Long, P. E., Dayvault, R., Karp, K., Marutzky, S., Metzler, D. R., Peacock, A., White, D. C., Lowe, M., and Lovley, D. R. (2003) Stimulating the in situ activity of *Geobacter* species to remove uranium from the groundwater of a uranium-contaminated aquifer, *Appl. Environ. Microbiol. 69*, 5884−5891.
3. Lovley, D. R. (2000) Fe(III) and Mn(IV) reduction, in *Environmental microbe-metal interactions* (Lovley, D. R., Ed.) pp 3−30, ASM Press, Washington, DC.
4. Lovley, D. R. (2001) Reduction of iron and humics in subsurface environments, in *Subsurface Microbiology and Biogeochemistry* (Fredrickson, J. K. F., and Fletcher, M., Eds.) pp 193−217, Wiley-Liss, Inc., New York.
5. Ortiz-Bernad, I., Anderson, R. T., Vrionis, H. A., and Lovley, D. R. (2004) Vanadium respiration by *Geobacter metallireducens*:

Novel strategy for in situ removal of vanadium from groundwater, *Appl. Environ. Microbiol. 70*, 3091−3095.
6. Rooney-Varga, J. N., Anderson, R. T., Fraga, J. L., Ringelberg, D., and Lovley, D. R. (1999) Microbial communities associated with anaerobic benzene degradation in a petroleum-contaminated aquifer, *Appl. Environ. Microbiol. 65*, 3056−3063.
7. Methé, B. A., Nelson, K. E., Eisen, J. A., Paulsen, I. T., Nelson, W., Heidelberg, J. F., Wu, D., Wu, M., Ward, N., Beanan, M. J., Dodson, R. J., Madupu, R., Brinkac, L. M., Daugherty, S. C., DeBoy, R. T., Durkin, A. S., Gwinn, M., Kolonay, J. F., Sullivan, S. A., Haft, D. H., Selengut, J., Davidsen, T. M., Zafar, N., White, O., Tran, B., Romero, C., Forberger, H. A., Weidman, J., Khouri, H., Feldblyum, T. V., Utterback, T. R., Van Aken, S. E., Lovley, D. R., and Fraser, C. M. (2003) Genome of *Geobacter sulfurreducens*: Metal reduction in subsurface environments, *Science 302* 1967−1969.
8. Butler, J. E., Kaufmann, F., Coppi, M. V., Nunez, C., and Lovley, D. R. (2004) MacA, a diheme *c*-type cytochrome involved in Fe(III) reduction by *Geobacter sulfurreducens*, *J. Bacteriol. 186*, 4042−4045.
9. Leang, C., Coppi, M. V., and Lovley, D. R. (2003) OmcB, a *c*-type polyheme cytochrome, involved in Fe(III) reduction in *Geobacter sulfurreducens*, *J. Bacteriol. 185*, 2096−2103.
10. Lloyd, J. R., Leang, C., Hodges Myerson, A. L., Coppi, M. V., Cuifo, S., Methe, B., Sandler, S. J., and Lovley, D. R. (2003) Biochemical and genetic characterization of PpcA, a periplasmic *c*-type cytochrome in *Geobacter sulfurreducens*, *Biochem. J. 369*, 153−161.
11. Kim, B. C., Qian, X., Leang, C., Coppi, M. V., and Lovley, D. R. (2006) Two putative c-type multiheme cytochromes required for the expression of OmcB, an outer membrane protein essential for optimal Fe(III) reduction in *Geobacter sulfurreducens*, *J. Bacteriol. 188*, 3138−3142.
12. Lovley, D. R., Holmes, D. E., and Nevin, K. P. (2004) Dissimilatory Fe(III) and Mn(IV) reduction, in *Advances in Microbial Physiology* (Poole, R. K., Ed.) Vol. 49, pp 219−286, Elsevier Academic, London.
13. Mehta, T., Coppi, M. V., Childers, S. E., and Lovley, D. R. (2005) Outer Membrane *c*-Type Cytochromes Required for Fe(III) and Mn(IV) Oxide Reduction in *Geobacter sulfurreducens*, *Appl. Environ. Microbiol. 71*, 8634−8641.
14. Lovley, D. R. (2006) Bug juice: Harvesting electricity with microorganisms, *Nat. Rev. Microbiol. 4*, 497−508.
15. Pokkuluri, P. R., Londer, Y. Y., Duke, N. E. C., Long, W. C., and Schiffer, M. (2004) Family of cytochrome c_7-type proteins from *Geobacter sulfurreducens*: Structure of one cytochrome c_7 at 1.45 Å resolution, *Biochemistry 43*, 849−859.
16. Pessanha, M., Londer, Y. Y., Long, W. C., Erickson, J., Pokkuluri, P. R., Schiffer, M., and Salgueiro, C. A. (2004) Redox Characterization of *Geobacter sulfurreducens* cytochrome c_7: Physiological relevance of the conserved residue F15 probed by site-specific mutagenesis, *Biochemistry 43*, 9909−9917.
17. Probst, I., Bruschi, M., Pfennig, N., and Le Gall, J. (1977) Cytochrome $c_{551.5}$ (c_7) from *Desulfuromonas acetoxidans*, *Biochim. Biophys. Acta 460*, 58−64.
18. Czjzek, M., Arnoux, P., Haser, R., and Shepard, W. (2001) Structure of cytochrome c_7 from *Desulfuromonas acetoxidans* at 9 Å resolution, *Acta Crystallogr. D57*, 670−678.
19. Coutinho, I. B., Turner, D. L., Ming, Y. L., LeGall, J., and Xavier, A. V. (1996) Structure of the three-haem core of cytochrome $c_{551.5}$ determined by ^{1}H NMR, *J. Biol. Inorg. Chem. 1*, 305−311.
20. Bento, I., Matias, P. M., Baptista, A. M., da Costa, P. N., van Dongen, W. M., Saraiva, L. M., Schneider, T. R., Soares, C. M., and Carrondo, M. A. (2004) Molecular basis for redox-Bohr and cooperative effects in cytochrome c_3 from *Desulfovibrio desulfuricans* ATCC 27774: Crystallographic and modeling studies of oxidized and reduced high-resolution structures at pH 7.6, *Proteins 54*, 135−152.
21. Correia, I. J., Paquete, C. M., Louro, R. O., Catarino, T., Turner, D. L., and Xavier, A. V. (2002) Thermodynamic and kinetic characterization of trihaem cytochrome c_3 from *Desulfuromonas acetoxidans*, *Eur. J. Biochem. 269*, 5722−5730.
22. Londer, Y. Y., Pokkuluri, P. R., Tiede, D. M., and Schiffer, M. (2002) Production and preliminary characterization of a recombinant triheme cytochrome c_7 from *Geobacter sulfurreducens* in *Escherichia coli*, *Biochim. Biophys. Acta 1554*, 202−211.
23. Seeliger, S., Cord-Ruwisch, R., and Schink, B. (1998) A periplasmic and extracellular *c*-type cytochrome of *Geobacter sulfurreducens* acts as a ferric iron reductase and as an electron carrier to other acceptors or to partner bacteria, *J. Bacteriol. 180*, 686−691.
24. Louro, R. O., Catarino, T., LeGall, J., Turner, D. L., and Xavier, A. V. (2001) Cooperativity between electrons and protons in a monomeric cytochrome c_3: The importance of mechano-chemical coupling for energy transduction, *ChemBioChem 2*, 831−837.
25. Pessanha, M., Louro, R. O., Correia, I. J., Rothery, E. L., Pankhurst, K. L., Reid, G. A., Chapman, S. K., Turner, D. L., and Salgueiro, C. A. (2003) Thermodynamic characterization of a tetrahaem cytochrome isolated from a facultative aerobic bacterium, *Shewanella frigidimarina*: A putative redox model for flavocytochrome c_3, *Biochem. J. 370*, 489−495.
26. Correia, I. J., Paquete, C. M., Coelho, A., Almeida, C. C., Catarino, T., Louro, R. O., Frazão, C., Saraiva, L. M., Carrondo, M. A., Turner, D. L., and Xavier, A. V. (2004) Proton-assisted two-electron transfer in natural variants of tetraheme cytochromes from *Desulfomicrobium* sp., *J. Biol. Chem. 279*, 52227−52237.
27. Salgueiro, C. A., da Costa, P. N., Turner, D. L., Messias, A. C., van Dongen, W. M., Saraiva, L. M., and Xavier, A. V. (2001) Effect of hydrogen-bond networks in controlling reduction potentials in *Desulfovibrio vulgaris* (Hildenborough) cytochrome c_3 probed by site-specific mutagenesis, *Biochemistry 40*, 9709−9716.
28. Pereira, P. M., Pacheco, I., Turner, D. L., and Louro, R. O. (2002) Structure-function relationship in type II cytochrome c_3 from *Desulfovibrio africanus*: A novel function in a familiar heme core, *J. Biol. Inorg. Chem. 7*, 815−822.
29. Santos, H., Moura, J. J. G., Moura, I., LeGall, J., and Xavier, A. V. (1984) NMR studies of electron transfer mechanisms in a protein with interacting redox centres: *Desulfovibrio gigas* cytochrome c_3, *Eur. J. Biochem. 141*, 283−296.
30. Salgueiro, C. A., Turner, D. L., Santos, H., LeGall, J., and Xavier, A. V. (1992) Assignment of the redox potentials to the four haems in *Desulfovibrio vulgaris* cytochrome c_3 by 2D-NMR, *FEBS Lett. 314*, 155−158.
31. Turner, D. L., Salgueiro, C. A., Catarino, T., LeGall, J., and Xavier, A. V. (1996) NMR studies of cooperativity in the tetrahaem cytochrome c_3 from *Desulfovibrio vulgaris*, *Eur. J. Biochem. 241*, 723−731.
32. Dolla, A., Blanchard, L., Guerlesquin, F., and Bruschi, M. (1994) The protein moiety modulates the redox potential in cytochromes *c*, *Biochimie 76*, 471−479.
33. Louro, R. O., Catarino, T., Paquete, C. M., and Turner, D. L. (2004) Distance dependence of interactions between charged centres in proteins with common structural features, *FEBS Lett. 576*, 77−80.
34. Brennan, L., Turner, D. L., Messias, A. C., Teodoro, M. L., LeGall, J., Santos, H., and Xavier, A. V. (2000) Structural basis for the network of functional cooperativities in cytochrome c_3 from *Desulfovibrio gigas*: Solution structures of the oxidized and reduced states, *J. Mol. Biol. 298*, 61−82.
35. Salgueiro, C. A., Turner, D. L., and Xavier, A. V. (1997) Use of paramagnetic NMR probes for structural analysis in cytochrome c_3 from *Desulfovibrio vulgaris*, *Eur. J. Biochem. 244*, 721−734.
36. Louro, R. O., Catarino, T., Turner, D. L., Piçarra-Pereira, M. A., Pacheco, I., LeGall, J., and Xavier, A. V. (1998) Functional and mechanistic studies of cytochrome c_3 from *Desulfovibrio gigas*: Thermodynamics of a "proton thruster", *Biochemistry 37*, 15808−15815.
37. Saraiva, L. M., Salgueiro, C. A., da Costa, P. N., Messias, A. C., LeGall, J., van Dongen, W. M. A. M., and Xavier, A. V. (1998) Replacement of lysine 45 by uncharged residues modulates the redox-Bohr effect in tetraheme cytochrome c_3 of *Desulfovibrio vulgaris* (Hildenborough), *Biochemistry 37*, 12160−12165.
38. Assfalg, M., Bertini, I., Bruschi, M., Michel, C., and Turano, P. (2002) The metal reductase activity of some multiheme cytochromes c: NMR structural characterization of the reduction of chromium(VI) to chromium(III) by cytochrome c_7, *Proc. Natl. Acad. Sci. U.S.A. 99*, 9750−9754.
39. Mahadevan, R., Bond, D. R., Butler, J. E., Esteve-Nunez, A., Coppi, M. V., Palsson, B. O., Schilling, C. H., and Lovley, D. R. (2006) Characterization of metabolism in the Fe(III)-reducing organism *Geobacter sulfurreducens* by constraint-based modeling, *Appl. Environ. Microbiol. 72*, 1558−1568.

BI061394V